Controlling the morphology in epoxy/thermoplastic systems

Eléonore Mathis, Marie-Laure Michon, Claude Billaud, Caroll Vergelati, Nigel Clarke, Jacques Jestin, Didier Long

Controlling the morphology in epoxy/thermoplastic systems

Eléonore Mathis[1], Marie-Laure Michon[2], Claude Billaud[2,3], Caroll Vergelati[1], Nigel Clarke[4], Jacques Jestin[5], Didier R. Long[1,6*]

[1]LPMA, Laboratoire des polymères et Matériaux Avancés, UMR 5268 Solvay/CNRS, Solvay in Axel'One, 87 avenue des Frères Perrets CS 70061 69192, Saint-Fons, France

[2]Solvay Research and Innovation, 87 avenue des Frères Perret CS 70061 69192, Saint-Fons, France

[3]Solvay Composite Materials, R420 The Wilton Centre, Redcar TS10 4RF, UK

[4]University of Sheffield, Department of Physics and Astronomy, Sheffield S3 7RH, UK

[5]Laboratoire Léon Brillouin, Bât 563 CEA Saclay, 91191 Gif sur Yvette Cedex, France

[6]Univ. Lyon, CNRS, INSA Lyon, Université Claude Bernard Lyon 1, MATEIS, UMR5510, 69100 Villeurbanne, France

Abstract

Thermosets are frequently toughened by a high-T_g thermoplastic (TP). Blend morphologies, obtained by curing induced phase separation with scales of a few hundreds of nanometers are relevant for high-performance applications, but no quantitative description for obtaining these morphologies exist yet. We propose such a quantitative approach for predicting and controlling the final morphology. The key is the degree of curing and the corresponding T_g of the blend and of both phases when phase separation takes place. It is controlled by the Flory interaction parameter χ of the constituents and their respective T_g's. We show that if phase separation takes place too early during curing, the T_g is too low and morphologies grow to reach sizes of a few micrometers, or more. Our study of different systems allows us to propose the relevant range of Flory interaction parameter χ and temperature window T- T_g for which the sizes of interest may be obtained. Our work opens the way for devising thermoplastics-thermosets couples with the appropriate affinity and T_gs in order to make blends with tailored morphologies.

1. Introduction

Thermosets and their fiber-reinforced composites are more and more used for replacing metals in high-performance applications in aerospace or automotive industries. A significant property is the strength-to-weight ratio which is more than 50 times higher when compared to steel [1]. Composite materials are high-strength and high-modulus fibers embedded in a polymer matrix. Epoxy prepolymers cured with an amine are often chosen for composite applications because of their high stiffness, good processability and good adhesion with the reinforcing fibers. The choice of epoxy resin of high functionality is attractive to obtain a material with a high T_g and a high crosslink density for which the strength and the stiffness are improved as well as the thermal resistance [2-4]. Nevertheless they are inherently brittle. They must be toughened to achieve good damage and impact resistance. The choice of a high-T_g

thermoplastic as toughening agent is judicious to improve epoxy resin toughness without a reduction in other properties such as the elastic modulus and the chemical resistance [5]. The soluble thermoplastic technology was used to prepare the epoxy-TP blends. Initially soluble in the thermoset precursors, the TP phase separates during curing through spinodal decomposition [6-8]. Using this method, Bucknall and Partridge [9] showed that epoxy resins could be toughened with polyethersulfones. It was shown subsequently that a co-continuous morphology of a few hundreds of nanometers could significantly increase the fracture toughness of these blends [10-12].

Despite decades of research, the desired morphologies with length scale of a few hundred of nanometers are obtained empirically only. No systematic method to do so has been proposed and established yet for controlling these morphologies. The parameters (curing temperature, chemical affinity between the constituents, molar mass of the polymer, glass transition temperature of the constituents,…) have only been identified at a qualitative level, but no quantitative description of their effects on the final morphologies has been proposed. The aim of this manuscript is to propose such a quantitative approach. It allows for predicting quantitatively the final morphologies as a function of these parameters and to devise a systematic method for obtaining the desired final morphologies of these blends, with the relevant length scales.

Numerous authors have shown that the thermoplastic content has a primary effect on morphology [9, 13-22]. Both co-continuous and sea-island morphologies have been observed to develop by spinodal decomposition in epoxy/TP blends [23-29]. The presence of reactive end-groups on the thermoplastic (such as amino groups) may favor the miscibility of the TP with the epoxy precursors and so delay phase separation [10, 15]. Other studies observed that when the thermoplastic molecular mass is increased, the phase separation occurs earlier in the curing process. This may lead to a small-sized particle or possibly to a phase-inverted morphology [4, 13, 19, 30, 31]. In addition, the viscosity of the different species that compose the blend influences system mobility and hence the final morphology [12, 13, 21, 32-34].

Some studies used *in situ* scattering methods showing an intensity peak that evolves during spinodal decomposition. Based on a consideration of viscoelastic relaxation [35], they discuss dynamic asymmetric phase separation, due to the T_g differences between epoxy and TP components [25, 26, 36]. An important consideration mentioned is that the TP acts as a slow dynamic component (high T_g) whereas epoxy acts as a fast dynamic component (low T_g). Emmerson [4] also noted that the TP content and the TP T_g influenced the diffusion coefficient for phase separation, and therefore the morphology growth rate. The resin and the curing agent may act as plasticizer and strongly influence the mobility of the separated phases: when curing reaction evolves, kinetics of phase separation decrease [9, 37]. The specific role of the T_g was not further investigated.

The final morphology is dictated by the epoxy monomers, specifically their structure, viscosity and relative miscibility with the TP [2, 9]. The influence of the epoxy affinity with the TP has not been studied in detail. Although different parameters have been assessed and a variety of systems characterized, no predictive model for the control of morphology in epoxy/TP systems has been discussed to date [5, 22, 38].

Systems with a low glass transition temperature and for which the phase separation occurs early, the phase separation may be described by standard spinodal decomposition with a high value of the diffusion coefficient leading to large morphologies in the final state of a few microns or more. Otherwise, if phase separation occurs at a later stage of the cure cycle, the T_g may have sufficiently increased to induce a slowing down of diffusion. The final morphologies are smaller and may be in the desired range for the application. For better controlling the final morphologies of these systems, one needs then to describe the phase separation process when it is coupled with the increase of the glass transition temperature during the curing process.

We propose in this manuscript a predictive approach for the morphology control, based on the parameters that we determine as the first order of influence. First, we study the miscibility of the constituents to determine the onset of phase separation. To follow, the T_g of the systems under study is determined as a function of TP content and epoxy conversion. Then, we show how the temperature difference between the process temperature and the T_g of the system, which depends on the degree of curing, determines the kinetics of phase separation. We study the final morphologies using electron microscopy and neutron scattering. The scattering experiments allow us to determine the size of the phases but not at this stage their compositions as there is one more unknown variable than equations. Two critical points are highlighted: the onset of phase separation related to the Flory interaction parameter, and the kinetics of phase separation related to the T_g and the epoxy conversion during phase separation. Finally, we show how describing the kinetics of phase separation allows for the determination of the compositions of the TP-rich phase and of the epoxy-rich phase. This methodology provides the keys to tailor materials for high-performance applications.

Two epoxy/TP systems are studied. Their morphologies were described in a previous paper through electron microscopy, dynamic mechanical thermal analysis and small-angle neutron scattering data [39]. They consist of one epoxy monomer (TGAP or TGDDM) cured with a 4, 4'- DDS. Two stoichiometry ratios are studied: 0.9 and 1.15. The resins are modified with 15 wt% of PES-5003P (Sumitomo), a high-T_g polyethersulfone (232 °C) with reactive end-group. The system composed of TGDDM presents small morphologies of about 20 nm width. The system with TGAP exhibits co-continuous morphologies with 300 nm scale in width.

The manuscript is structured as follows. Materials and methods are presented in Section 2. The complete methodology is then described in Section 3. Phase diagrams are constructed in Section 3.2 and phase separation process discussed in Section 3.3. The determination of the T_g of the TP-rich and epoxy-rich phases is described in Section 3.4. Small-angle neutron scattering results are analyzed in Section 3.5. In Section 4, all the results are discussed and we propose a mechanism of phase separation which allows us to describe the morphologies obtained and their sizes. We discuss how to obtain sizes in the range of a few hundred of nanometers.

2. Materials and methods

2.1. Materials and sample preparation

The epoxy resin precursors were kindly supplied by Huntsman Advanced Materials, Basel (Switzerland): triglycidyl-p-aminophenol (TGAP, Araldite MY0510) with a Tg of -40.9 °C, tetraglycidyl diaminodiphenylmethane (TGDDM, Araldite MY721) with a T_g of -15.0 °C and 4, 4'-diaminodiphenylsulfone (4, 4'-DDS, Aradur 9664-1). The thermoplastic used is a hydroxyl-functionalized polyethersulfone (PES, PES-5003P from Sumitomo) with a number average molecular weight of 24 000 g.mol–1 and a T_g of 232 °C (Figure 1).

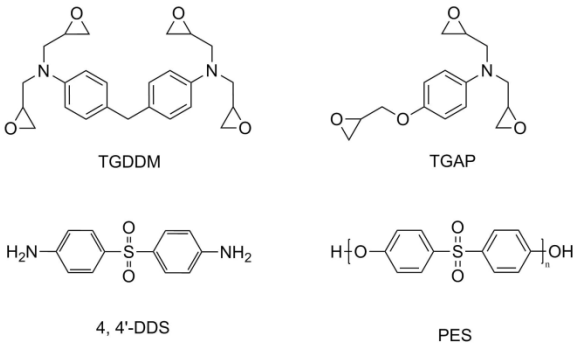

Figure 1 Structure of the different components studied.

Four systems are formulated. System A1 is prepared by mixing TGDDM with 4, 4'-DDS at a stoichiometric ratio (NH/Ep) of 0.9 and system B1 is prepared by mixing TGAP with 4, 4'-DDS at a stoichiometric ratio (NH/Ep) of 0.9. Their analogous systems A2 and B2 are prepared with a stoichiometric ratio (NH/Ep) of 1.15. The polyethersulfone content is fixed at 15 weight percent (wt %) for all systems. The formulations are gathered in Table S1.

Systems are prepared by dissolving first the thermoplastic in the epoxy monomer of choice at 140 °C; 4 hours are needed for the TGDDM systems while only 2 hours are sufficient for the TGAP systems. The 4, 4'-DDS curing agent is then added to the homogenized blend of epoxy and TP at 120°C. The mixture is further stirred to achieve a partial dissolution of the 4, 4'- DDS. Before curing, the samples are degassed under vacuum at 90 °C for 2 hours. Finally for all systems, similar cure profiles are used with first a temperature ramp of 1 °C.min^{-1} up to 180 °C and a plateau maintained at 180 °C to achieve the resin full cure. For all systems, we checked that no reaction occurs during degassing and that the DDS is dissolved, by running DSC analyses on non-degassed and degassed samples. The final degree of cure is determined by running DSC analyses on the cured sample and by comparing the residual heat flow to the total heat flow determined from the degassed samples. It evolves from 90 % for TGDDM-systems to 95 % for TGAP-systems.

2.2. Characterization of the dynamics properties of pure PES thermoplastic

Small strain dynamic oscillatory shear measurements are performed using a RDA3 rheometer from TA instrument in plate-plate geometry. Samples were dried at 120 °C under vacuum for 28h (water residue < 900 ppm). The dried polymer powder is then placed between the two plates of the plate-plate

geometry. The temperature is controlled with the assistance of liquid nitrogen. Strain sweeps are performed at each temperature to confirm the linear viscoelastic regime of the measurements. Frequency sweeps are performed at a constant temperature, within a range of 0.16 to 82 Hz. For each sample, at each temperature, two consecutive frequency sweep tests are run to assert the thermal stability of the material. The time-temperature superposition was applied to build a master curve. A vertical and horizontal shift is applied on frequency sweeps at all temperatures to a reference temperature. The horizontal shift factor is fitted using a WLF (Equation 1) and WLF parameters are then determined at the T_g of the thermoplastic [40, 41].

$$\log a_T = \frac{-C_1(T - T_g)}{C_2 + T - T_g} \quad (1)$$

Where C_1 and C_2 values at T_g are 11.42 and 29.18, respectively.

2.3. Determination of interaction parameters

The Flory interaction parameters for the studied systems were calculated in a previous paper [39] by means of the Hoy method [42] to tabulate the group contributions. They will be used for the determination of the free energy of the blend and the construction of the phase diagrams. For each system, the interaction parameters were calculated in the initial system and then for epoxy polymers in formation, i.e. up to three epoxies bonded with three curing agents. For TGAP-system the interaction parameter first slightly evolves and then stabilized at a value of 0.03. For TGDDM-system the interaction parameter stabilized at a value of 0.27.

2.4. Characterization of the morphology and thermo-mechanical properties

Characterizations have been performed and discussed in a previous paper [39]. The morphology of cured samples was studied by electron microscopy. According to the size of the morphology, different methods were used: Scanning Electron Microscopy (SEM) with a Zeiss Ultra 55 microscope or Transmission Electron Microscopy (TEM) with a Jeol 1400. Dynamic mechanical thermal analysis (DMTA) measurements were performed on a rectangular bar (40 x 10 x 2-5 mm^3) of cured resins, using a rheometer Scientific analyzer RSAG2 (TA Instruments) using the three-point bending method. Relaxation temperatures are determined as the peak maximum of tanδ plot. Dynamic scanning calorimetry analyses were performed on a Q2000 differential Scanning Calorimeter (TA Instruments) to determine the kinetics of epoxy curing. Dynamic rheological measurements were conducted by using an oscillation rheometer (ARES-G2 rheometer, TA Instruments) equipped with disposable parallel plate geometry of 25 mm in diameter. The gel point is determined as the crossover of four tanδ curves collected at different frequencies.

2.5. Investigation on the T_g: T_g measurement of non-reactive binary blends and T_g measurement of epoxy network along curing process.

Non-reactive binary blends of epoxy/ TP or curing agent/ TP are prepared with different content of TP. Their T_g are measured by DSC during the second heating ramp at 10 °C.min^{-1}.

In another experiment, the evolution of the T_g as a function of epoxy conversion is measured. Two neat resins (without thermoplastic) are synthesized with TGAP and with TGDDM at a stoichiometry of 0.9.

They are cured with 4, 4'- DDS with the same process as systems A and B. Samples are quenched at different times corresponding to different process temperature (according to a 1° C.min^{-1} temperature ramp). Their T_g are measured by DSC on the first heating ramp at 10 °C.min^{-1}. In parallel, DSC experiments of these two neat resins have been performed at 1 °C.min^{-1} (ramp of the curing process) so that it is possible to correlate the process temperature at which the sample has been quenched to the epoxy conversion.

2.6. Small-angle neutron scattering study

Small-angle neutron scattering (SANS) experiments are carried out on the D11 beam-line at the Institute Laue Langevin (ILL, Grenoble, France). Three configurations (sample-to-detector distance/wavelength) are used: 5.5 m/5.3Å, 28m/5.3Å, 37m/12 Å, covering a range of scattering vector q from 5×10^{-4} to 1×10^{-1} Å^{-1} [43]. The samples of the four formulations are prepared in a home-made mold consisting of aluminum rectangle of 23.75 mm width, 46 mm high and 1.5 mm thick, with a hole of 20 mm diameter centered at 13 mm high. A position is kept empty to measure the background intensity to subtract. For each sample, the three scattering curves corresponding to each configuration are normalized by the thickness and transmission and by incident beam intensity. The three curves are rescaled in absolute unit intensity. The incoherent intensity is subtracted and the coherent scattered intensity I(q) is obtained. The differential scattering cross section per unit volume of sample reads (Equation 2) [43, 44]:

$$I(q) = \frac{d\sigma}{d\Omega}(per\ unit\ volume) = N(\Delta\rho)^2V^2P(q) \quad (2)$$

where *I(q)* is the scattering intensity (cm^{-1}), q is the scattering vector (Å^{-1}), N is the number of scattering objects per unit volume (cm^{-3}), $(\Delta\rho)$ is the scattering length density contrast (SLD) (cm^{-2}), V is the volume of scattering objects (cm^3). $P(q)$ is the form factor, the objects are uncorrelated so that the structure factor is equal to one.

The scattering length density contrast ($\Delta\rho$) is the difference of scattering length density between two phases of a material. The coherent scattering length density of a material is defined in Equation 3:

$$\rho = \left(\sum n_i b_i\right)\frac{d\ N_A}{M_w} \quad (3)$$

where n_i is the number of an isotope in the component, $b_i$is the coherent scattering length of an isotope, d is the density of a material (g.cm^{-3}), N_A is the Avogadro number (mol^{-1}) and $M_w$is the molar mass of the component (g.mol^{-1}).

The scattering length density (SLD) contrast between phase 1 and phase 2 is then defined in Equation 4.

$$\Delta\rho = \rho_1 - \rho_2 \quad (4)$$

The theoretical coherent scattering length densities of the different species are calculated using the neutron scattering lengths for isotopes (periodic table provided by the NIST Centre for Neutron Research [45]) and given in Table S2. The theoretical coherent SLD contrasts (which assumes pure phases) in the four systems are given in Table S3.

Beaucage et al. [46] have proposed a global unified scattering function which approximates the scattering of a particle on the Guinier and Porod region. For spherical particles, it is written as in Equation 5:

$$I(q) = G\left(\exp\left(\frac{-q^2R^2}{5}\right) + 4.5\ \mathrm{BB}\frac{\left(\mathrm{erf}\left(\frac{qR}{\sqrt{10}}\right)\right)^{12}}{(qR)^4} \right) \quad (5)$$

where erf(x) [47] is the error function. BB is the Beaucage fitting parameter (dimensionless). R is the object radius (cm) and q is the scattering vector ($Å^{-1}$). G is a prefactor (cm^{-1}) given by:

$$G = \emptyset\ (1-\emptyset)\mathrm{V}(\Delta\ \rho)^2 \quad (6)$$

where $\emptyset$ is the volume fraction of the objects, V the volume of the objects (cm^3). Note that the Beaucage model does not take into account the possible correlation of position of the diffusing objects [46].

3. Results

3.1. Observation of phase separation

After curing, the morphologies of all formulations were characterized by SEM, TEM, DMTA and neutron-scattering as reported previously [39]; it can be summarized as follows. For A1 and A2, the presence of objects with 20 nm in diameter was determined. Both systems B showed quasi co-continuous morphologies. In system B1, the average width of the PES-rich domains was about 300 nm. For the system B2 cured with an amine excess, it was about 200 nm. Further interpretation of the neutron-scattering data will be done in Part 3.5.

3.2. Miscibility of the constituents

The reaction-induced phase separation in the resins is interpreted through the Flory-Huggins theory of polymer blend for which the Gibbs free enthalpy per monomer reads (Equation 7):

$$G = \mathrm{kT}\left[\frac{\emptyset_{TP}}{N_{TP}}\ln\emptyset_{TP} + \frac{(1-\emptyset_{TP})}{N_{Epoxy}}\ln(1-\emptyset_{TP}) + \chi_{TP,Epoxy}\emptyset_{TP}(1-\emptyset_{TP})\right] \quad (7)$$

where $\emptyset_{TP}$ and $(1-\emptyset_{TP})$ are the volume fractions of the TP and of the epoxy respectively, N_{TP} and N_{Epoxy} are the polymerization degrees of each specie, $\chi_{TP,Epoxy}$ is the Flory interaction parameter between monomer units of each specie, i.e. TP and epoxy.

The epoxy size N_{Epoxy} starts from 1 and then increases during epoxy curing [48]. A phase diagram can be drawn for each N_{Epoxy}. Above a certain value of N_{Epoxy} the system becomes unstable; the second derivative of the free enthalpy is negative, and it phase separates [4, 22, 49, 50]. After phase separation, curing continues, and the two components become less and less compatible. The compositions of the

two phases are given by the construction of the common tangent as illustrated in Figure 2, for system A (left) and system B (right).

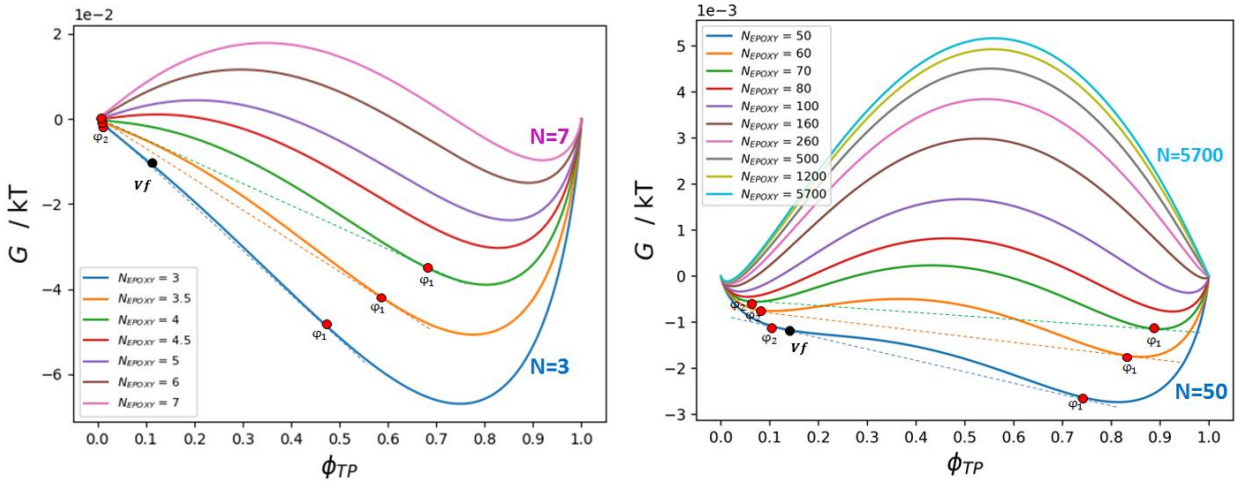

Figure 2 Evolution of free enthalpy of TP/epoxy blend as a function of the TP volume fraction. For TGDDM-system (left), N_{Epoxy} value varies from 3 to 7, and for TGAP-system (right), N_{Epoxy} value varies from 50 to 5700. Vf is the initial volume fraction of TP. It separates in two phases with concentrations $\varphi_1$and φ_2. When N_{Epoxy} increases, φ_1 increases and φ_2 decreases.

Systems A become unstable at a relatively low epoxy conversion (N_{Epoxy}=5) and phase separates with TP volume fractions in TP-phase (φ_1) and in epoxy-phase (φ_2) equal to 0.48 and 0, respectively. Systems B are stable until a high degree of conversion (N_{Epoxy}=50) when it phase separates with TP volume fractions in TP-phase (φ_1) and in epoxy-phase (φ_2) equal to 0.74 and 0.12, respectively. These are the compositions which would correspond to a system at equilibrium with the current epoxy conversion, i.e. N_{Epoxy}.

3.3. Experimental determination of the phase separation onset and end

In a previous paper [39], the epoxy cure reaction of the systems was characterized by dynamic rheology and DSC analysis. The combination of the two techniques allows for the determination of the temperature at the gel point (based on Winter's criterion, i.e. tanδ crossover in a multifrequency test [51]), and the corresponding epoxy conversion (Table 1, columns 2 and 3). It is believed that gelation prevents the morphology from evolving [12, 52, 53], so we consider gelation as the end of the phase separation. The onset of phase separation was inferred from dynamic rheology for B1 and B2 as a change of slope of the viscosity profiles, and the corresponding epoxy conversion was determined (Table 1, columns 4 and 5). No deviation of viscosity was observed for systems A1 and A2. With the construction of the phase diagram (Part 3.2), it is possible to determine the epoxy size (N) for which the systems phase separate. The corresponding epoxy conversion and temperature are determined and given in columns 6, 7 and 8 in Table 1.

Table 1 Characteristics of the phase separation and of the gel point of systems A and B.

	Determination of gel point temperature by rheology and degree of cure by DSC. *In parenthesis, we put the theoretical value obtained by the Flory-Stockmayer equation.*		**Determination of onset of phase separation temperature (rheology) and degree of cure (DSC)**		**Determination of onset of phase separation by phase diagram study**		
System	GP temperature +/- 1 (°C)	Degree of cure at GP *(Flory-Stockmayer GP [39])*	Curing temperature at phase separation +/- 1 (°C)	Degree of cure at phase separation	N_{Epoxy} at phase separation	Degree of cure at phase separation	Curing temperature at phase separation +/- 1 (°C)
A1	173	0.33 *(0.32)*	not observed	/	3	0.13	156
A2	167	0.42 *(0.36)*	not observed	/	3	0.16	151
B1	166	0.49 *(0.39)*	161	0.41	50	0.41	162
B2	157	0.47 *(0.44)*	153	0.38	50	0.40	154

Note that for systems B1 and B2, there is a good similarity between epoxy conversion determined by dynamic rheology and determined through the phase diagram study. Based on such observations, the degree of cure values at phase separation determined by the phase diagram construction will be considered in the discussion for all systems.

3.4. Determination of the T_g of the TP-rich and epoxy-rich phase during phase separation

To understand the influence of the dynamic behavior of the systems A1 and B1 on the phase separation kinetics, the T_g of the TP-rich phase and of the epoxy-rich phase during the curing process has to be determined. The TP-rich phase is composed of TP (high T_g) and epoxy monomers or oligomers (low T_g). The T_g varies during the curing process because of the growth of the epoxy oligomers.

It was not possible to determine directly by DSC the T_g of the TP-rich phase and the T_g of the epoxy-rich phase mostly because the signal displays by the T_g of the TP-rich phase was too weak (in classic or modulated-DSC) and at the end of the cure reaction, the T_g of the two components are too close to be discriminated. Thus, a step-by-step DSC methodology is proposed here to approximate the T_g of the TP-rich phase and of the epoxy-rich phase all along the curing process. First, the T_g of binary non-reactive TP/epoxy blend is measured for different epoxy contents. The second step is to measure the T_g of neat epoxy resin (without TP) as a function of epoxy conversion. Finally, results obtained from the first and second steps are combined. The T_g of the TP-rich phase is plotted both as a function of the TP-rich phase content in epoxy and as a function of the epoxy conversion.

The affinity of the TP with the epoxy monomer is good enough to obtain homogeneous blends upon mixing in temperature for a broad range of composition. TGDDM and TGAP epoxy monomers have a low T_g of -15 °C and -41 °C respectively. In comparison, the TP has a T_g of 232 °C. Epoxy monomers play a role of plasticizer.

The glass transition temperature of thermoplastic-epoxy blends are measured by DSC experiments for different compositions, up to 40 wt% of TP in epoxy monomers (Figure S1). Larger TP contents were not considered because of a dramatic increase in viscosity. The T_g of blends made with a higher TP content (above 40 wt%) was obtained by extrapolation. Considering an adjustable k parameter, Couchman-based equation (Equation 8) [54] was found to be adequate as observed in Figure S1.

$$T_g = \frac{T_{g1} w_1 + k T_{g2} w_2}{w_1 + k w_2} \quad (8)$$

T_g is the glass transition temperature of the blend, T_{g1}, T_{g2}, w_1 and w_2 are the glass transition temperatures and the mass fractions of components 1 and 2, respectively. k is an adjustable parameter. For each system the T_g values observed evolved from the T_g of the pure TP, 232 °C down to the T_g of the pure epoxy monomer (-15°C and -41 °C for TGDDM and TGAP respectively). It decreases with the content of epoxy monomer. k values of 2.68 and 5.48 are determined for systems A1 and B1, respectively (Figure S1).

The epoxy conversion dependence of T_g of neat epoxy can be represented by using the Di Benedetto's equation modified by Pascault and Williams [55] (Equation 9):

$$\frac{T_g - T_{g0}}{T_{g\infty} - T_{g0}} = \frac{\lambda\, \alpha}{1 - (1 - \lambda)\, \alpha} \quad (9)$$

where α is the epoxy conversion, T_{g0} and $T_{g\infty}$ are the glass transition temperatures (°C or °K) of the uncured and the fully cured system, respectively. The experimental data are fitted with λ as an adjustable parameter as it was done by Rosetti [10]. λ is found to be 0.95 and 1.10 for system A1 and B1 respectively (Figure S2). Overall, throughout the resin curing, the T_g values of TGDDM network are 6 to 10 °C higher than the ones of TGAP network, at the same epoxy conversion.

The T_g values that evolve with epoxy conversion and the phase contents control the kinetics of phase separation process. So that, the results of the two studies (Figure S1 and Figure S2) are combined on a single graphic for calculating the evolution of T_g during phase separation and curing. The plots obtained for each system are displayed in Figure S3 for System A1 and in Figure 3 for System B1. This gives a continuum of T_g values for TP-rich phases and epoxy-rich phases for a range of blend composition, upon cure, by extrapolation. The T_g values of the neat resin recorded upon cure are placed on the y-axis for an abscissa of 1 in volume fraction of epoxy monomer (100 volume percent, 100 vol%). The T_g value of the pure TP can be indicated on the y-axis for an abscissa of 0 in volume fraction (0 vol%). A curve can be plotted between the two epoxy compositions 0 and 1. For each epoxy conversion, the curve between the two points is plotted by using Equation 8 (Couchman-based equation) with k=2.68 for TGDDM-system and k=5.48 for TGAP-system. We suppose that the same functions with the same k

parameters describe a same system prior to reaction and whilst it is curing. Each curve indicates the evolution of T_g of the epoxy/TP blend as a function of the composition, for a fixed epoxy conversion. Thus, the final graph represents the evolution of the T_g as a function of the volume fraction of epoxy monomer and of epoxy conversion. For a fix amount of epoxy monomer, the change in T_g value with the epoxy conversion increase can be read moving up from one curve to another.

In the systems of this study, phase separations occur, so that the T_g of the homogeneous system is read up to the epoxy conversion for which phase separation takes place (Figure 3 for system B1 and Figure S3 for system A1), from point 1 to 2). Then the T_g of the TP-rich phase and the T_g of the epoxy-rich phase can be read in the direction of the T_{g1} and T_{g2} arrows, respectively, by knowing the volume fraction of epoxy in each phase.

In the initial state, 13 %vol of TP are introduced which gives the initial point 1 (volume fraction TGDDM=0.87) for system A1 (Figure S3). Then the cure reaction begins and the T_g of the blend for the evolving epoxy conversion are read along the vertical line (black arrow between points 1 and 2) until it reaches the curve representing the epoxy conversion at phase separation. Due to poor compatibility between the constituents, phase separation occurs early at a low value for the degree of curing (α=0.13). After point 2, two phases coexist with a certain T_g which depends on the phase composition and on the epoxy conversion. When the phase separation process continues, the composition of each phase evolves towards those corresponding to thermodynamic equilibrium at the current epoxy conversion. The T_g of the TP-rich phase are read in the direction of the left arrow (T_{g1}) and the T_g of the epoxy-rich phase are read in the direction of the right arrow (T_{g2}). The positions of the left and right arrows are drawn arbitrarily on Figure S3 because we do not know the exact trajectory of the systems in the diagram, which will be discussed later.

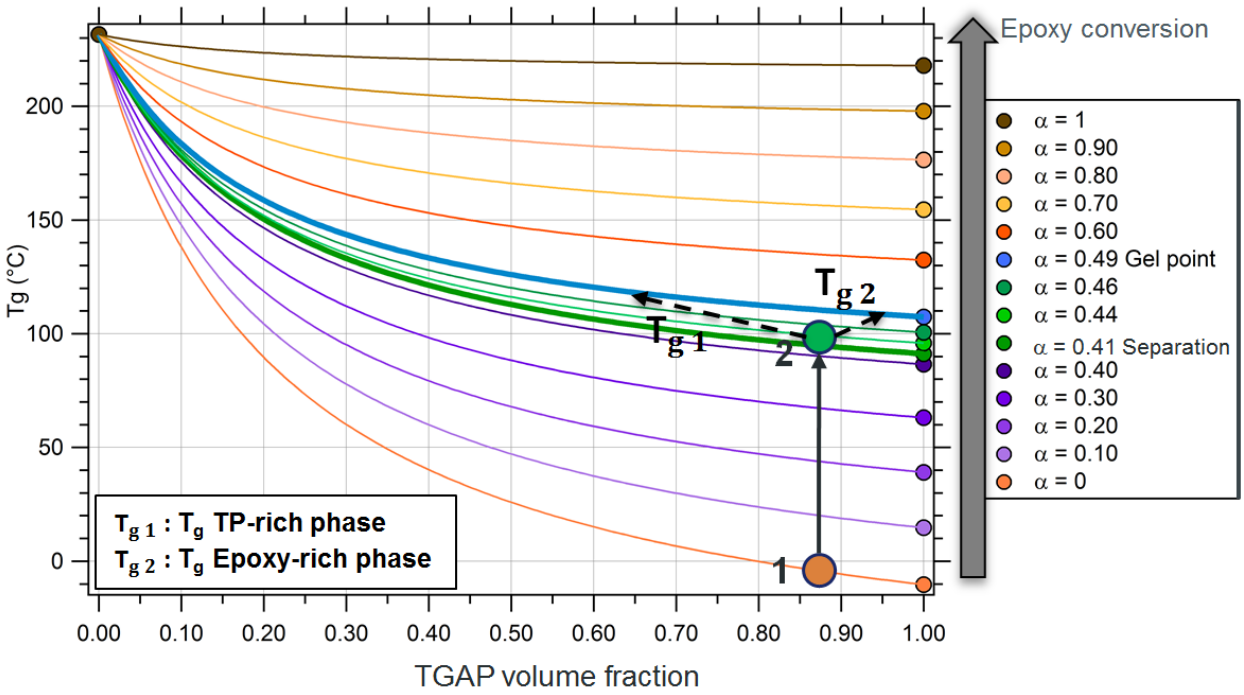

Figure 3 Evolution of the Tg during curing as a function of TGAP volume fraction, for system B1. Point 1 is the Tg of the homogeneous blend before curing. Point 2 is the Tg of the blend at phase separation. Tg1 is the Tg of the TP-rich phase, Tg2 is the Tg of the epoxy-rich phase. The arrows indicate the direction to read Tg1 and Tg2 but do not correspond to precise values.

For system B1 the T_g of the epoxy/TP blend can be read from Figure 3. The starting point 1 is 87 vol% of TGAP. The T_g of the blend increases (black arrow) up to point 2 which corresponds to the phase separation (α=0.41). Then two phases coexist and their respective T_g can be read along the direction of the T_{g1} (TP-rich phase) or T_{g2} (epoxy-rich phase) arrows.

Note that in this study, we always work with a same temperature ramp but different temperature cycle would lead to different onset of phase separation. The methodological approach can be easily adapted to other curing process.

3.5. Small-Angle neutron scattering for the determination of morphology size and composition

Small-Angle neutron scattering measurements are performed on cured systems to determine the exact size of the morphologies and to access the phase compositions in the final system. From the obtained 2D patterns, the scattering intensities are integrated over the isotropic system.

For systems A1 and A2, no clear morphology was observed by SEM or TEM but the DMTA indicated the occurrence of phase separation. The size and shape of the developed morphologies were detected by neutron scattering measurements (Figure S4); a slope of q^{-4} and the Guinier plateau on the low-q indicating the presence of 3D objects with defined interface [46]. The experimental data are fitted with the Beaucage global unified equation for a sphere (Equation 5).

The variables to consider are: ξ the average diameter (2R) of TP-rich phase, BB the Beaucage parameter, $\varphi_{2\mathrm{Epoxy}}$ the volume fraction of epoxy in the epoxy-rich phase, $\varphi_{1\mathrm{TP}}$ the volume fraction of TP in the TP-rich phase and $\emptyset_1$ the volume fraction of TP-rich phase. ξ is fixed by the position of the peak, and BB is a fixed dimensionless number which is here set equal to 3. The last three parameters are related together for the global TP mass conservation through Equation 10.

$$\emptyset_1 = \frac{Vf - 1 + \varphi_{2\mathrm{Epoxy}}}{\varphi_{1\mathrm{TP}} - 1 + \varphi_{2\mathrm{Epoxy}}} \quad (10)$$

V_f is the initial volume fraction of TP introduced. For both systems, V_f=0.13 which corresponds to the TP content of 15 wt%.

Under the hypothesis that the phases are pure thermoplastic and pure epoxy, respectively, the calculated scattered intensity is orders of magnitude too high as compared to experimental results: the two phases are not pure and their compositions need to be determined. The parameters which fit the neutron scattering data of cured system A1 and which satisfy Equation 10 are given in Table S4. Because there are three variables ($\varphi_{2\mathrm{Epoxy}}$, $\emptyset_1$, $\varphi_{1\mathrm{TP}}$) for only two equations (Equations 5 and 10), a continuum of solutions exist, which we exemplify with solutions from A to M in Table S4.

The size of the morphology determined by neutron scattering is 19.5 nm. The Beaucage parameter (BB) which makes the link between the Guinier and Porod regions is set equal to 3. The volume fraction of epoxy in epoxy-rich phase ranges from 1 (pure phase) to 0.88. The smaller the epoxy fraction in the epoxy-rich phase ($\varphi_{2\mathrm{Epoxy}}$) is, the larger the TP fraction in the TP-rich phase ($\varphi_{1\mathrm{TP}}$) is. Note that the possible $\varphi_{1\mathrm{TP}}$ values vary from 0.18 to 0.70 (Table S4), which indicates a large presence of epoxy in the TP-rich phase. The maximum amount of TP in the TP-rich phase considered is 0.70 which corresponds to a volume fraction of thermoplastic rich phase of 2 % only.

While A1 is a TGDDM-system at a stoichiometry of 0.9, A2 is at stoichiometry of 1.15. Nevertheless, the intensity scattered by system A2 is the same as for system A1 which indicates that similar morphologies are obtained. The same parameters are also used to fit the experimental data of cured system A2 and the same solutions (A to M) are found.

For systems B1 and B2, co-continuous morphologies were observed by SEM and TEM. The analysis of neutron scattering curves permits to determine quantitatively the morphology size and the composition of the two phases. The scattered intensities of systems B1 and B2 are given in Figure 4. They indicate the presence of two populations of morphologies: one in the low-q range (coarse size) and the other in the high-q range (small size). Note that due to the presence of two bumps in the scattering curve, it is not possible to fit the results with only one broad distribution such as a power law. Hence, two scenarios are discussed for systems B. A schematic of the morphology suggested in the two scenarios is given in Figure 5.

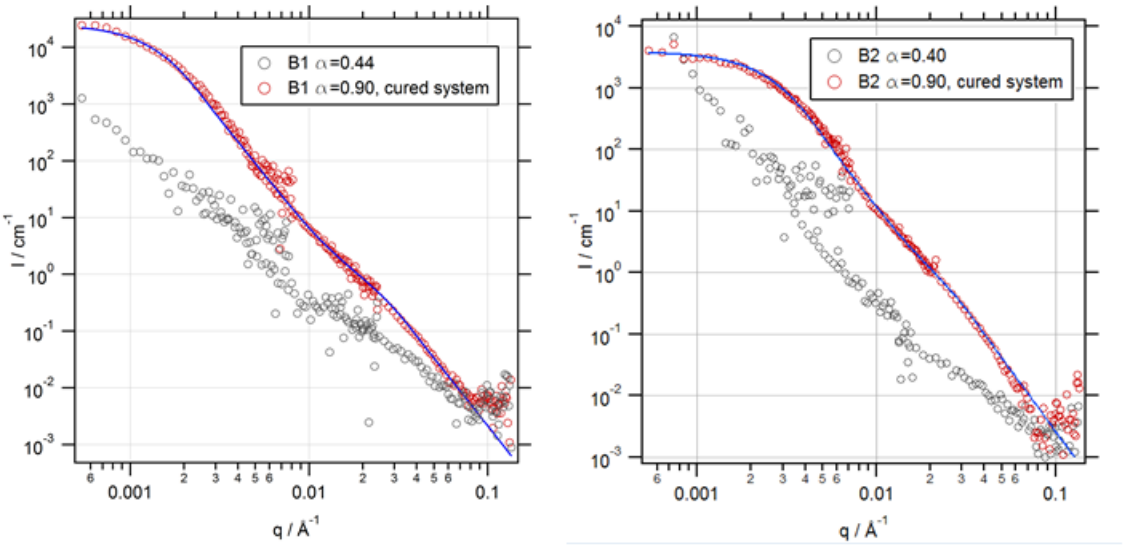

Figure 4 SANS intensity of systems B1 (left) and B2 (right), for α=0.44 and 0.40, respectively (grey) and for α=0.90 (red) and the fitting curves (blue).

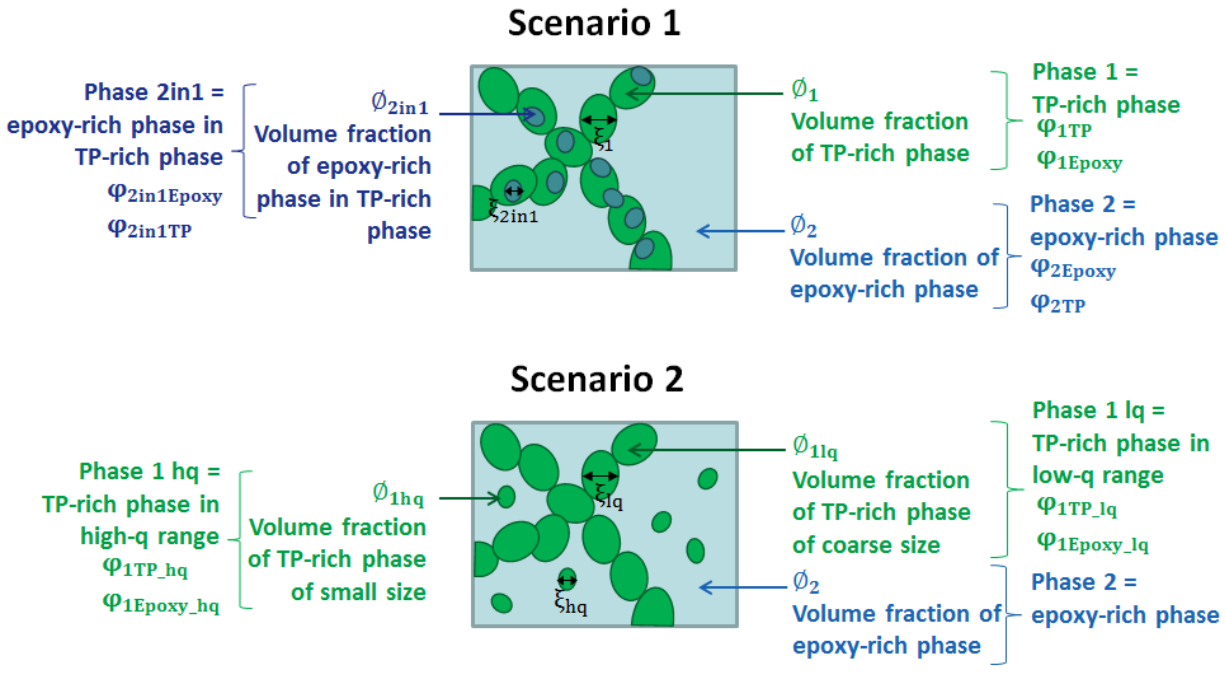

Figure 5 Schematized morphology in system B, Scenario 1 and Scenario 2. In green are the compositions of the TP-rich phases. In blue are the compositions of the epoxy-rich phase.

In both scenarios, the population with the coarsest size (low-q range) corresponds to the TP-rich phase. In the Scenario 1, the second population of morphology corresponds to sub-inclusions of epoxy-rich

phase inside the coarse TP-morphology; whereas in the Scenario 2, the second population corresponds to small TP-rich phases.

Only Scenario 1 permits the reproduction of the neutron data. The variables are ξ_1 the average characteristic size of TP-rich objects, $\varphi_{1\mathrm{TP}}$ the volume fraction of TP in TP-rich phase, $\emptyset_1$ the volume fraction of TP-rich objects, $\varphi_{2\mathrm{Epoxy}}$ the volume fraction of epoxy in the epoxy-rich phase, $\xi_{2\mathrm{in1}}$ the characteristic size of the epoxy-rich objects included in TP-rich phase, $\varphi_{2\mathrm{in1Epoxy}}$ the volume fraction of epoxy in epoxy-rich objects included in the TP-rich phase, $\emptyset_{2\mathrm{in1}}$ the volume fraction of epoxy-rich objects in TP-rich phase, and BB1 and BBhq the Beaucage parameters. The conservation of the TP is given by Equation 11 and Equation 12 for low-q range and high-q range respectively:

$$\emptyset_1 = \frac{Vf - 1 + \varphi_{2\mathrm{Epoxy}}}{\varphi_{1\mathrm{TP}} - 1 + \varphi_{2\mathrm{Epoxy}}} \quad (11)$$

And

$$\emptyset_{2\mathrm{in1}} = \frac{Vf - \varphi_{1\mathrm{TP}} \times \emptyset_1}{(1 - \varphi_{2\mathrm{in1Epoxy}})} \quad (12)$$

Where V_f is the initial volume fraction of TP introduced (V_f= 0.13).

The experimental data are fitted with the Beaucage global unified equation (Equation 5) for two populations of spheres. A co-continuous structure can be understood as percolated spheres where its width is considered as the sphere's diameter.

Scenario 2 does not allow fitting the neutron experimental data with respect to mass conservation; it results in curves with too low intensity as compared to the experimental results. Moreover, scenario 2 does not seem probable regarding the very low content of TP that remains in the epoxy-rich phase after phase separation according to the phase diagram of System B.

Thus, we use Scenario 1, in which the large quantity of epoxy remaining in the TP-rich phase continues to branch until a certain conversion for which there is (secondary) phase separation. This results in epoxy-rich nodules in TP-rich phase, as also observed in some systems in the literature [8, 21, 56]. The parameters which best fit the experimental data of system B1 and take account of the relations between the parameters (Equations 11 and 12) are given in Table S5. Again a continuum of different solutions exists, which we exemplify from A to J. The TP-rich morphology of system B1 fits with a lengthscale of 340 nm. Results of the fitting indicate epoxy-rich nodules (sub-inclusion) of 22 nm in diameter. For primary (low-q) or secondary morphology (high-q), the Beaucage parameter (BB1 and BBhq) is found to be equal to 4. The volume fraction of epoxy in the epoxy-rich phase ($\varphi_{2\mathrm{Epoxy}}$) is between 0.99 and 0.90. The fraction of TP in the TP-rich phase ($\varphi_{1\mathrm{TP}}$) may cover a wide range of composition: from 0.36 to 0.92 which corresponds to a volume fraction of TP-rich phase from 0.34 to 0.04. Concerning the sub-inclusion morphology, it is highly concentrated in epoxy: from 0.95 to 0.74 ($\varphi_{2\mathrm{in1Epoxy}}$) and represents 0.13 to 0.37 ($\emptyset_{2\mathrm{in1}}$) of the volume of the TP-rich phase in which it is included.

Different solutions also exist to fit the experimental data of system B2 with scenario 1, in the same range of compositions but with smaller TP-rich nodules (180 nm).

Note that the intensity scattered at different stage of the phase separation was also measured (from α=0.20 to α=0.33 and from α=0.44 to α=0.49 for A1 and B1 respectively) with the aim of accessing the detailed kinetics of phase separation, but no significant evolution of the peak position or intensity could be measured. The contrast between both phases may not be strong enough before the final stages of phase separation. Note that neither the neutron scattering experiments, nor the electron microscopic observations allowed us to observe morphologies at intermediate steps of partial curing.

Our results validate the presence of sub-inclusions in systems B, which was suggested by microscopy images but without certainty. Also, neutron scattering results give detailed information on the compositions of TP-rich and epoxy-rich phases (and the sub-inclusions in the case of Systems B) but further analysis are needed to determine the one solution that describes the system. The mechanisms of phase separation for each system are discussed in the following section.

4. Interpretation and discussion

4.1. Kinetics of phase separation and diffusion process

In a previous work [38], we described the morphologies observed by electron microscopy but we did not provide explanations regarding the phase separation process which we do here. The growth of the morphology is fixed by different parameters: the onset of phase separation, the end of separation which is often determined as the gel point that fixed the morphology, and the kinetics of growth during the elapsed time [22]. The characteristics of phase separation of the four systems, in term of epoxy conversion and process temperature at phase separation and at gel point, are summarized in Table 1 above.

In the early stage of spinodal decomposition in polymer blends, an initial demixing length scale is favored according to Cahn-Hilliard theory [57, 58]. Then the growth rate reaches a maximum [4, 36, 59] and then during the later stage of spinodal decomposition the kinetics of phase separation is described by Ostwald-ripening mechanism [60, 61]. The time of growth is directly related to the final size morphology. For constant diffusion coefficient, domains size grows proportionally to $t^{1/3}$ (Equation 13) [61, 62]:

$$\xi \approx (N\, D\, a\, t)^{1/3} \qquad (13)$$

ξ is the size (m), N is the number of monomers per chain (here, N=103), D is the diffusion coefficient of the polymer ($m^2.s^{-1}$), a is the monomer size ($a=10^{-9}$m), and t is the time for phase separation (s). D may be considered as constant if the phase separation process takes place well above the T_g, e.g. at about T_g + 100 °C [62]. Then, the dynamics is very fast, with a diffusion coefficient typically around 10^{-13} $m^2.s^{-1}$. For an experimental time of 10^3 s, the characteristic size calculated with Equation 13 is around 2 µm, which is not the scale of morphology that we aim for. Indeed, we work at temperatures closer to T_g. To explain the obtained nanoscale morphology, we need to take into account the effect of the T_g on the spinodal decomposition process.

For systems A1 and B1 respectively, the value of the T_g of the epoxy/TP blend throughout the cure reaction can be determined from Figure 3 and Figure S3. From the moment of phase separation (point 2), the T_g of the TP-rich phase can be read to the left while the T_g of the epoxy-rich phase can be read to the right, when knowing the epoxy amount (abscissa).

We assume that the diffusion dynamics is set by the slowest component [62, 63], thus we aim to determine the monomeric relaxation times of the TP slow component in both the TP-rich and the epoxy-rich phases. The Williams-Landel-Ferry (WLF) [40, 41] can be used to determine the TP monomeric relaxation times in both phases. We then proceed to shift the curve when considering a phase with a different T_g. We use the same WLF coefficients C_1 and C_2 as those determined for the pure TP. To determine the monomeric relaxation time τ_α, the WLF curve is plotted for various T_g of the TP-rich or epoxy-rich phase (**Figure 6**).

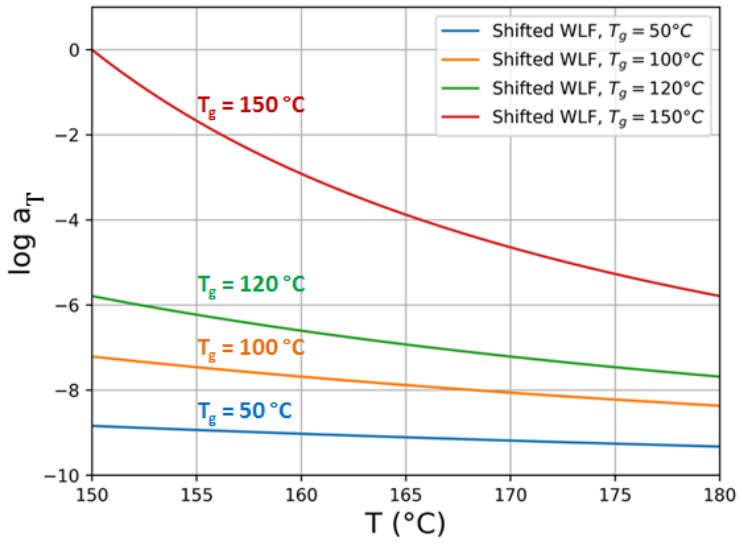

Figure 6 WLF curves for several examples of TP-rich or epoxy-rich phase having four different Tg (50, 100, 120, 150 °C)

For example, if the phase has a T_g of 100 °C (orange curve) and the process temperature is 155 °C, so that log a_T= -7.5 and the monomer relaxation time of the TP (τ_α) is 3×10^{-6} s ($log\ a_T = log\left(\frac{\tau_\alpha}{\tau_{ref}}\right)$). Once τ_α is determined, the diffusion coefficient D_{TP} (m².s^{-1}) can be estimated by using Equation 14 [64]:

$$D_{TP} = \frac{a^2 \times N_e}{\tau_\alpha \times N^2} \quad (14)$$

Where a is the monomer size (typically a=10^{-9} m), τ_α(s) is the monomer relaxation time of the thermoplastic, N is the number of monomer unit (N=103) and N_e is the entanglement number (N_e=34).

N_e is determined as M_e/M_0 ratio with M_e the entanglement mass determined on the dynamic rheology curve with the plateau modulus G_N^0 as $M_e = \rho RT/G_N^0$ [41], and M_0 the molecular mass of the monomer unit.

4.2. Proposition of mechanisms for phase separation and kinetics of morphology growth

According to the phase diagram, phase separation starts when N=3 for A1 which corresponds to a degree of cure of 0.13, whilst it starts when N=50 for B1, which corresponds to a degree of cure of 0.41, which is also consistent with rheological studies.

The growth of the morphology characteristic size is controlled by the diffusion of the TP in the epoxy-rich phase as illustrated in the scheme below (**Figure 7**). The polymer chains diffuse in the epoxy-rich phase to gather at the boundaries of the high-T_g thermoplastic-rich phase. Consequently, the domains of the thermoplastic-rich phase grow.

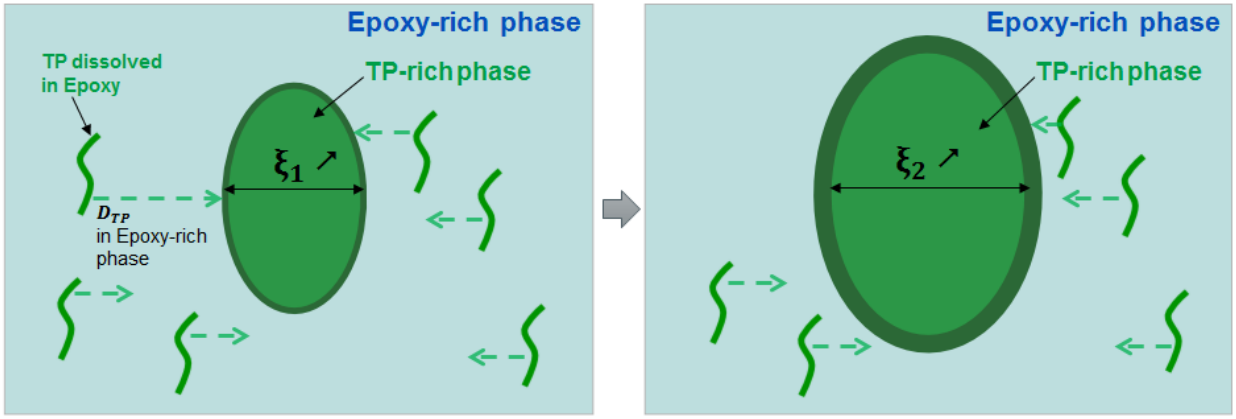

Figure 7 Scheme of the growth of TP-rich phase by diffusion of the TP through the epoxy-rich phase, $\xi_2 > \xi_1$

On the other hand, the increase of the concentration of the TP-domain is driven by the diffusion of the TP within the TP-rich phase. The TP diffuses from the interface of the TP-rich phase to the inside of the morphology so that the average concentration of the TP-rich phase increases.

4.2.1. Systems B1 (TGAP-based system)

Based on neutron scattering results and microscopy observation, System B1 exhibits co-continuous morphology of 340 nm in width. We calculate the morphology size and its composition by using the methodology based on the determination of the T_g. As a first approximation, we monitor the T_g increase with TP content on the curve at the onset of phase separation (α=0.41, corresponding to N = 50). The co-continuous structure grows by diffusion of the TP through the epoxy-rich phase (Figure 7). At the onset of separation, the epoxy-rich phase contains 12% of TP as read from Figure 2. This composition corresponds to a T_g of 92 °C (Figure 3), so that T- T_g = 70 °C (when α=0.41, $T_{process}$=162 °C). The monomer relaxation time is calculated with Equation 1: $\tau_\alpha = 1\times10^{-6}$ s. The corresponding diffusion coefficient is 3.8×10^{-15} m².s^{-1} (Equation 14). In the time elapsed between the onset of phase separation and the gel point of 4 min, the TP-rich structure can grow from 5 to 450 nm as calculated with Equation 13. This length scale is comparable to the one observed by microscopy and small-angle neutron scattering (340 nm). The parameters are summarized in Table 2.a.

Table 2 Parameters for the phase separation process description

Table 2.a Phase separation in system B1

α	$T_{process}$ +/- 1 (°C)	φ_{2TP}	φ_{2Epoxy}	$T_{g,\ epoxy\text{-}rich\ phase}$ +/- 1 (°C)	τ_α (s)	D_{TP} ($m^2.s^{-1}$)	Δt (s)	ξ (m)
0.41	162	0.12	0.88	92	1×10^{-6}	3.8×10^{-15}	234	4.5×10^{-7}

Table 2.b Calculation of TP concentration in the TP-rich phase in system B1

α	$T_{process}$ +/- 1 (°C)	ξ (m)	Δt (s)	D_{TP} ($m^2.s^{-1}$)	τ_α (s)	$T_{g,\ TP\text{-}rich\ phase}$ +/- 1 (°C)	φ_{1TP}
0.41	162	2.2×10^{-7}	234	4.5×10^{-16}	1×10^{-5}	112	0.53

The increase of TP concentration in the TP-rich phase is driven by the diffusion of the TP though the TP-domains. Indeed, the more the TP-rich phase is concentrated (during the process), the higher the TP monomer relaxation time and the smaller the diffusion coefficient. Thus, more time is needed for the TP to diffuse from the interface to the inside morphology (~220 nm). This process is limited by the time for phase separation (230 s), which allows us to determine the maximum composition of the TP-rich phase. The value of the T_g of the TP-rich phase that enables a sufficient mobility (D_{TP}) to diffuse 220 nm (that is radius of the considered morphology), is calculated with Equations 1, 13 and 14. The required diffusion coefficient is 4.5×10^{-16} $m^2.s^{-1}$; corresponding to a monomer relaxation time of 1×10^{-5} s. At the curing process of 162 °C, this monomer relaxation time corresponds to a T_g of the TP-rich phase of 112 °C. That corresponds to about 53 vol% of TP when reading on the α=0.41 curve of the T_g diagram (**Erreur ! Source du renvoi introuvable.**3). The parameters resulting from the phase separation kinetics analysis are summarized in Table 2.b. This value of 53 vol% of TP in TP-rich phase (φ_{1TP}) allows choosing Solution F from the possible neutron scattering fits (Table S5). Thus, we can deduce the volume ratio of TP-rich phase to be about 14% ($\emptyset_1$). This proportion seems in accordance with the images analysis of SEM morphology. Also, there is about 94 vol% of epoxy in the epoxy-rich phase (φ_{2Epoxy}). Moreover, solution F gives the proportion and composition of the small epoxy-inclusions inside the TP-rich phase. They occupy about 29 vol% of the TP-rich phase ($\emptyset_{2in1}$) and are composed of 82 vol% of epoxy ($\varphi_{2in1epoxy}$).

Note that only about 60% of the TP introduced initially has phase separated, the rest remains in the epoxy-rich phase. It is indeed limited by the kinetics of diffusion whereas thermodynamic equilibrium corresponds to larger composition differences.

4.2.2. Systems A1 (TGDDM-based system)

Based on the neutron scattering results, A1 systems display very small morphologies of 20 nm. Phase separation occurs when N=3, α=0.13 as determined on the phase diagram. The growth of the morphology in principle is controlled by the diffusion of the TP through the epoxy-rich phase (Figure 7), which depends significantly on the T_g of the epoxy-rich phase, and on its composition. Throughout the

curing process and for any TP amount, the T_g of the TGDDM-rich phase is very low as compared to the curing temperature, as can be read on Figure S3. Even if the onset of phase separation could occur some degree of conversion later because of the compatibilization of the TP with the epoxy through its reactive end-group, the T_g of the TGDDM-rich phase remains low at low epoxy conversion. For example, at phase separation (α=0.13, $T_{process}$= 156 °C), there is at the very maximum 13% of TP in the epoxy-rich phase (initial TP volume fraction). The T_g of the epoxy-rich phase is of 47 °C (T- T_g = 109 °C), the monomer relaxation time is at most 1×10^{-7} s and the corresponding diffusion coefficient is 3×10^{-14} $m^2.s^{-1}$ (Equations 1 and 14). Thus the morphology should reach 1.5 μm (Equation 13) whereas a 20 nm size was determined by neutron-scattering. Values discussed here regarding the scale of the morphologies and their compositions for systems A are gathered in Table S6.a. and Table S6.b.

When conversion evolves, the mobility decreases but T- T_g is always greater than 80 °C. Thus, at any time, the monomer relaxation time is shorter than 4×10^{-7} s so that the diffusion of TP through the epoxy-phase is fast and the size should be larger than 600 nm (Equation 13) in a few minutes. Thus, the mechanism of morphology growth by diffusion through the epoxy-rich phase does not permit to explain the 20 nm size of morphology in A1.

Regarding the final morphology of 20 nm for A1, we deduce from our results that the process is arrested at an early stage of spinodal decomposition. We propose that this is due to the reaction of the TP-end group with the epoxy. When phase separation occurs (T=156 °C), the morphology can first slightly grow (from 5 to 20 nm). However, the hydroxyl end-group of the TP immediately reacts with the epoxy at the interface between the two phases. Indeed, at around 150 °C the –OH-epoxy reaction is fast [10]. An epoxy-TP block copolymer forms a dense brush around the TP-rich phase. Moreover, it is favored because of a high incompatibility between TP and epoxy (χ=0.27). The organization in micelles blocks the penetration of the TP inside the TP-rich phase. Thus phase separation is arrested [65]. The same effect of the reactive end-group was observed by different authors [10, 56, 66] for epoxy/TP blends. When TP had reactive end-groups (-NH_2 or -OH), the characteristic sizes obtained were of the order of 20 to 90 nm depending on the epoxy monomer.

In term of TP-rich phase composition, the concentration is driven by the diffusion of the TP in the TP-rich phase. As for system B1, we determine for A1 the T_g of the TP-rich phase which provides a sufficient diffusion of the TP from the interface to the inside morphology (length around 10 nm). It is calculated with Equations 1, 13 and 14 through the determination of the diffusion coefficient and monomer relaxation time. For T= 156 °C at phase separation, the T_g of the TP-rich phase is 148 °C. This corresponds to 78% of TP in the TP-rich phase when reading on the α=0.13 curve (Figure S3). This value of 78 vol% of TP in TP-rich phase ($\varphi_{1\mathrm{TP}}$) allows choosing Solution M from neutron scattering (Table S4). Thus, we can deduce that the volume ratio of TP-rich phase is only 2% ($\emptyset_1$). Also, there is about 88 vol% of epoxy in the epoxy-rich phase ($\varphi_{2\mathrm{Epoxy}}$).

Let us note that only about 10% of the TP introduced initially is within the TP-rich phase by the end of the process. Most of the TP remains trapped within the epoxy-rich phase: the phase separation is not advanced at all. Our interpretation is that the reaction of the TP-end group with epoxy occurs probably on the same time scale as that of the epoxy reaction with amine which is slow in these systems. So, in

parallel TP-end group branch and the epoxy network evolves. The TP that has already reacted can be solubilized inside the epoxy-rich phase (because it has increased their affinity with epoxy) or even becomes part of the network. The TP that has not yet reacted phase separates and forms a TP-rich phase. The TP at the interface of this phase then reacts as well and form a block TP-epoxy barrier. In this way, the morphology only attains 20 nm sizes and is poorly concentrated: the phase separation is frustrated. This could explain why no morphology was observed by electronic microscopy.

System B1 has faster network formation kinetics and we propose that the TP-end group reaction is too slow in comparison so that it does not come into play during the phase separation mechanism. The TP-rich phase is formed and grows up to the gel point. Because the elapsed time for phase separation is short (4 min), the structure remains co-continuous and percolation-to-cluster mechanism does not occur. The determination of the kinetics of TGAP-TP reaction and TGDDM-TP reaction compared to epoxy curing kinetics and phase separation would be interesting to validate this hypothesis.

4.2.3. Systems A2 (TGDDM-based) and B2 (TGAP-based) composed of an excess of curing agent

Systems A2 and B2 are cured with an excess of curing agent (NH/Ep=1.15). In both cases, small molecules of unreacted curing agent may migrate into the TP-rich phase because of their good affinity [67]. The same scattering intensity was obtained for A2 compared to A1, so that the morphology size and composition are similar with a TP-rich morphology of 20 nm in width. For both A1 and A2 systems, the phase separation is frustrated because the epoxy reacts faster with TP end-group than with amines. The excess of amines in A2 do not change the kinetics competition.

In B2 system, the morphology obtained exhibits a 180 nm length scale which is about a factor of two smaller than in B1, that we attribute to a decrease of phase separation kinetics. First, as already discussed in a previous article, the viscosity of the blend is higher in B2 than in B1 [39] during the whole curing process because of the presence of amines in excess. Thus, whereas the epoxy conversions at phase separation are similar (α=0.41 and α=0.40 for B1 and B2, respectively), the T_g of the epoxy-rich phase is higher in B2 than in system B1 (based on results from rheology experiments). In addition, the process temperature at phase separation is lower due to faster curing kinetics (almost 10 °C lower than in B1). As a consequence of the two aspects (higher T_g and lower T), the T- T_g value is smaller and the mobility of the thermoplastic is reduced. So, the phase separation kinetics is slower than in System B1 (diffusion of TP in epoxy-rich phase), which leads to a smaller morphology size.

4.2.4. Further discussion

In the literature, some studies observed the influence of the dynamic properties of epoxy/TP systems on final morphologies. Gan et al. [26] studied a DGEBA-system modified with PEI of different molecular mass. Scanning Electron Microscopy (SEM) images of the cured sample indicated large PEI-structure (some microns) in a continuous epoxy phase close to a co-continuous structure. It was observed that the final size decreased with the decrease of the molecular mass. Phase separation was measured to occur later in the process for the system with the lowest PEI molecular mass. Although the epoxy conversion was not followed during the experiment, we can understand that the epoxy conversion at phase

separation was higher for the low molecular mass PEI. Based on our study, we deduce that the T_g of the epoxy-rich phase should be higher at phase separation for low molecular mass PEI systems, which results in a small final morphology.

Rico et al. [30] also showed the influence of the T_g but for phase-inverted structures. They studied DGEBA systems cured with diamine and a stoichiometry of 1 with a PS with low molecular weight and a PS with high molecular weight. For high TP amount, the size of epoxy nodules in continuous PS phase was smaller for the resin modified with TP of high molecular mass. We understand that the TP-phase had an increased T_g , so that T- T_g was smaller for high molecular mass TP systems. The diffusion coefficient was decreased so that the kinetics of epoxy domains was reduced.

The same authors [21] studied qualitatively the influence of the isothermal process temperature on the morphology of DGEBA-based systems. The authors characterized the systems but did not quantify the temperature window T- T_g that we can now use based on our study. For sea-island morphology the TP-nodules size decreased with an increase in the isothermal process temperature. They explained this based on the fact that the affinity between epoxy and TP increased when the temperature is increased. Thus, phase separation occurred at higher epoxy conversion. As a consequence, T- T_g at phase separation is smaller (assuming that the increase of T_g is the dominant effect as compared to the increase of curing temperature), because the T_g of the continuous epoxy-phase is higher as compared to previous systems. In contrast, in a phase-inverted morphology the epoxy-nodules size increased with an increase in the curing temperature. Indeed, the viscosity of the continuous TP-phase decreased because of a higher temperature, so that T- T_g is larger compared to systems at lower temperature: the diffusion is favored. The same influence can be understood in the work of Saalbrink et al. [33] where a temperature increase of 20 °C induced an increase of phase-inverted morphology size in DGEBA/PS systems. They confirmed that the gel time was kept the same regardless the curing temperature. It supports the main influence of the T_g of the continuous phase in final morphology, more than a possible influence of the epoxy curing kinetics. Note that we did not address the relationship between the shrinkage factor of the resin and the phase separation. It would be of interest in further investigations, as discussed in references [68-70].

We studied other formulated systems with the same approach that was proposed in this paper [71]. Most of the obtained morphologies attained the scale of 70 to 400 nm. In this case the spinodal decomposition was coupled with the T_g. The onset of phase separation occurred late during the epoxy conversion so that the epoxy-rich phase had a high T_g as compared with the process temperature. The variation of morphology size inside this category could be explained by a difference in T- T_g gap. The larger T- T_g was, the coarser was the morphology. According to the resulting size, T- T_g was between 40 and 60 °C, the monomer relaxation time was between 10^{-4} and 10^{-6} s and the diffusion coefficient between 10^{-17} and 10^{-15} $m^2.s^{-1}$. As Systems B1 and B2 in this paper, different systems modified with a TP with reactive end-group and cured at a 0.9 stoichiometry entered this category. For two other systems, morphologies of some microns (from 800 nm to 7 µm) were obtained. In these systems, phase separation occurred early during the curing process so that the T_g of the epoxy-rich phase was low and T- Tg > 100 °C, the diffusion coefficient was faster than 10^{-13} $m^2.s^{-1}$. A system modified with 20wt% of non-reactive TP entered this category. Also, a system cured with an excess of curing agent showed very

coarse morphology. Indeed, both epoxy-rich and TP-rich phases were plasticized by the presence of small unreacted molecules of curing agent, and thus their T_g were considerably reduced. Note that the elapsed time between the phase separation and the gel point for all systems was in the scale between 200 and 1000 s, so that even if it could influence marginally the size, it was not the main factor that controls the size scale. It is instead the value of T- T_g which is the main factor for controlling the kinetics of morphology growth.

This study gives new keys to control the final morphology in thermoplastic/thermoset blends. The standard description of spinodal decomposition is not relevant for the range of morphology sizes of a few hundred of nanometers. One needs to consider the increase of and the approach to the glass transition temperature of the system upon curing for accounting for the final morphology. The mobility of the phases is dictated by the amount of TP and by the advancement of epoxy conversion. It plays a crucial role on the final morphology size, more than the time elapsed between phase separation and gel point. We highlight the ways to control the onset of phase separation, based on interaction parameters determination, and to control the T_g during phase separation process, as well as the methodology to characterize it.

We propose a scheme (Figure 8) to localize the region of interest to reach the intended morphology of a few hundreds of nanometers, which can be done by tuning adequately the parameter χ and the T_g as compared to the curing temperature. The system (its initial T_g and the affinity between components) and the process temperature (T) have to be chosen to phase separate when T- T_g is around 60-70 °C. Here the scheme is drawn for a system with an initial T_g around 0 °C (epoxy + TP blend). As an example, the green crosses represent the system B1 studied in detail in this paper. It has an interaction parameter of χ = 0.03 and the phase separation occurs when T= 160 °C and T_g= 90 °C. With these conditions, a morphology of 300 nm is obtained. But if in a specific system, the affinity between the epoxy and the thermoplastic is not good with a high value of the Flory parameter (i.e. log 1/χ close to 1), one needs to work with a higher T_g epoxy (which will shift the scheme above), or to cure the system at a relatively low temperature. In these conditions, the early phase separation of this kind of system would occur in the targeted range: T- T_g = 70 °C. But according to the kinetics of epoxy curing, the temperature must be high enough to allow the curing so that the region of interest is rather located in the red zone drawn in the scheme.

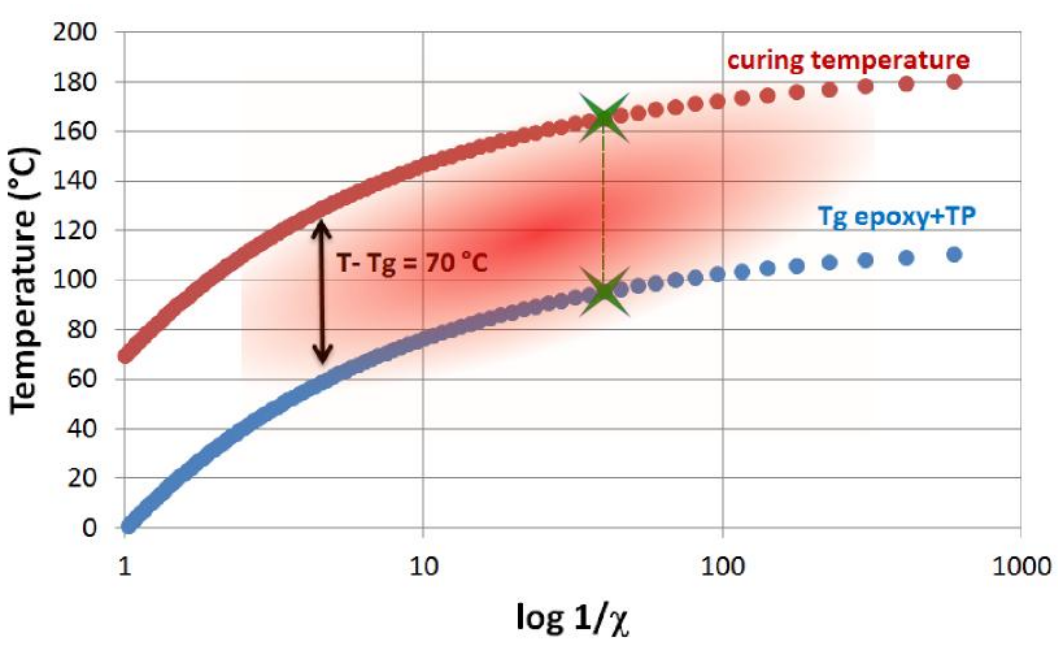

Figure 8 Temperature constraints (T, Tg) versus Flory interaction parameter. It represents the zone of interest to achieve morphology a few hundreds of nanometers. Here it is drawn for an initial Tg of the blend of 0 °C.

To complete the understanding of the phase separation mechanisms, other systems should be studied with the method discussed. Most of all, it would be interesting to vary independently the T_g of the components (TP or epoxy) and the affinity between TP and epoxy. According to these examples of avenues of research, a wide range of systems could then be understood in detail. In this way a more systematic control of the final morphology would be possible and would allow fine-tuning the high-performance mechanical properties.

5. Conclusions

We have identified the relevant parameters for controlling the final morphologies and sizes of thermoplastic/epoxy blends obtained by curing induced spinodal decomposition. The key is the glass transition temperature of the blends when phase separation takes place. We have shown how the latter is controlled by the affinity χ between the components, their respective glass transition temperatures and the curing temperature, which allows for predicting the final morphologies quantitatively. Morphologies of some hundreds of nanometers which are relevant for high-performance applications may be obtained when the glass transition temperature at phase separation is typically of order 70 °C. The difference $T\text{-}T_g$ at phase separation may be tuned by the affinity of the epoxy and the thermoplastic, or by tuning the curing temperature so that $T\text{-}T_g$ at phase separation remains in the targeted range. We have shown how coupling the dynamical description of phase separation and neutron scattering experiments allows also for determining the compositions of the thermoplastic-rich and epoxy-rich phases. Extension of this work may aim at more detailed experimental descriptions regarding morphology growth *e.g.* by performing *in situ* neutron scattering studies during curing. Future works will explore the appropriate phase space in the 2D space (T_g, χ) where T_g is the glass transition temperature

of the thermoplastic and χ the affinity between a thermoplastic and a given epoxy monomer, by varying independently these two parameters. Our work opens the way to designing thermoplastic-thermoset couples with the adequate affinity and T_g to obtain tailored morphologies and sizes.

Supporting Information

Materials preparation; neutron scattering; Tg's of the blend during curing; morphologies and composition (neutron scattering); morphology growth.

Acknowledgment

The authors thank the microscopy team of Solvay RIC-Lyon, particularly Pauline Grau and Clémence Abadie. They thank Sylvain Prévost and Ralf Schwein, scientists in the Institut Laue-Langevin for their collaboration in the neutron scattering experiments, at Institut Laue-Langevin, 71 avenue des Martyrs, CS 20156, 38042 Grenoble cedex 9, France.

[*] corresponding author. Email: didier.long@insa-lyon.fr

[1] Q. Guo, Thermosets: Structure, Properties and Applications, Woodhead Publishing Ltd, 2012.
[2] E.W.F. Jeremy O. Swanson, Steven M. Wand, Monoj Pramanik and James W. Rawlins Investigation of network development and properties in multifunctional epoxy resins using 3,3'-diaminodiphenylsulfone., (2010).
[3] K. Frank, C. Childers, D. Dutta, D. Gidley, M. Jackson, S. Ward, R. Maskell, J. Wiggins, Fluid uptake behavior of multifunctional epoxy blends, Polymer 54(1) (2013) 403-410.
[4] G.T. Emmerson, Phase separation and mechanical properties of epoxy/thermoplastic blends, Durham University, Durham University, 2003.
[5] J. Wang, R. Liu, X. Jian, Introduction to Epoxy/Thermoplastic Blends, 2017, pp. 429-458.
[6] R.J.J. Williams, B.A. Rozenberg, J.-P. Pascault, Reaction-induced phase separation in modified thermosetting polymers, Polymer Analysis Polymer Physics, Springer Berlin Heidelberg, Berlin, Heidelberg, 1997, pp. 95-156.
[7] J.-P. Pascault, Rubber- and thermoplastic-modified polymer networks. Phase separation process induced by polymerization and polycondensation, Macromolecular Symposia 93(1) (1995) 43-51.
[8] E. Girard-Reydet, H. Sautereau, J.P. Pascault, P. Keates, P. Navard, G. Thollet, G. Vigier, Reaction-induced phase separation mechanisms in modified thermosets, Polymer 39(11) (1998) 2269-2279.
[9] C.B. Bucknall, I.K. Partridge, Addition of polyethersulphone to epoxy resins, British Polymer Journal 15(1) (1983) 71-75.
[10] Y. Rosetti, P. Alcouffe, J.-P. Pascault, J.-F. Gérard, F. Lortie, Polyether Sulfone-Based Epoxy Toughening: From Micro- to Nano-Phase Separation via PES End-Chain Modification and Process Engineering, Materials (Basel, Switzerland) 11(10) (2018) 1960.
[11] M. Jiang, Y. Liu, C. Cheng, J. Zhou, B. Liu, M. Yu, H. Zhang, Enhanced mechanical and thermal properties of monocomponent high performance epoxy resin by blending with hydroxyl terminated polyethersulfone, Polymer Testing 69 (2018) 302-309.
[12] I. Martinez, L. Martin, A. Eceiza, P.A. Oyanguren, I. Mondragon, Phase separation in polysulfone-modified epoxy mixtures. Relationships between curing conditions, morphology and ultimate behavior, Polymer 41 (2000) 1027-1035.
[13] R. Sellak, Elaboration et caractérisation d'une résine thermodurcissable conductrice, Université du Maine, 2013.

[14] P. Oyanguren, M. Galante, K. Andromaque, P. Frontini, R. Williams, Development of bicontinuous morphologies in polysulfone–epoxy blends, Polymer 40(19) (1999) 5249-5255.
[15] I. Blanco, G. Cicala, O. Motta, A. Recca, Influence of a selected hardener on the phase separation in epoxy/thermoplastic polymer blends, Journal of Applied Polymer Science 94(1) (2004) 361-371.
[16] J.P. Pascault, R.J.J. Williams, Formulation and characterization of thermoset-thermoplastic blends, Polymer Blends Volume 1: Formulation (2001) 380-414.
[17] P.A. Oyanguren, C.C. Riccardi, R.J.J. Williams, I. Mondragon, Phase separation induced by a chain polymerization: Polysulfone-modified epoxy/anhydride systems, Journal of Polymer Science Part B: Polymer Physics 36(8) (1998) 1349-1359.
[18] Y. Zhang, F. Chen, W. Shi, Y. Liang, C.C. Han, Layered structure formation in the reaction-induced phase separation of epoxy/polysulfone blends., Elsevier (2010).
[19] M. Rico, C. Ramírez, B. Montero, J. Díez, J. López, Phase Diagram for a System of Polydisperse Components Consisting of the Precursor of an Epoxy/Diamine Thermoset and a Thermoplastic: Analysis Based on a Lattice Theory Model, Macromolecular Theory and Simulations 15(6) (2006) 487-496.
[20] J. López, C. Ramírez, M.J. Abad, L. Barral, J. Cano, F. Díez, Dynamic mechanical analysis of an epoxy/thermoplastic blend: polymerization-induced phase separation, Polymer International 51(10) (2002) 1100-1106.
[21] M. Rico, J. López, B. Montero, R. Bellas, Phase separation and morphology development in a thermoplastic-modified toughened epoxy, European Polymer Journal 48(10) (2012) 1660-1673.
[22] J.-P. Pascault, H. Sautereau, J. Verdu, R.J.J. Williams, Thermosetting polymers, CRC Press, Boca Raton, 2002.
[23] Z. Zhang, J. Cui, S. Li, K. Sun, W. Fan, Effect of Hydroxyl-Terminated Polyethersulfone on the Phase Separation of Polyetherimide-Modified Epoxy Resin, Macromolecular Chemistry and Physics 202(1) (2001) 126-132.
[24] P. Jyotishkumar, J. Koetz, B. Tiersch, V. Strehmel, C. Ozdilek, P. Moldenaers, R. Hassler, S. Thomas, Complex phase separation in poly(acrylonitrile-butadiene-styrene)-modified epoxy/4,4'-diaminodiphenyl sulfone blends: generation of new micro- and nanosubstructures, The journal of physical chemistry. B 113(16) (2009) 5418-30.
[25] W. Gan, Y. Yu, M. Wang, Q. Tao, S. Li, Viscoelastic Effects on the Phase Separation in Thermoplastics-Modified Epoxy Resin, Macromolecules 36(20) (2003) 7746-7751.
[26] W. Gan, W. Xiong, Y. Yu, S. Li, Effects of the molecular weight of poly(ether imide) on the viscoelastic phase separation of poly(ether imide)/epoxy blends, Journal of Applied Polymer Science 114(5) (2009) 3158-3167.
[27] P.A. Oyanguren, M.J. Galante, K. Andromaque, P.M. Frontini, R.J.J. Williams, Development of bicontinuous morphologies in polysulfone–epoxy blends, Polymer 40(19) (1999) 5249-5255.
[28] I. Martinez, M.D. Martin, A. Eceiza, P. Oyanguren, I. Mondragno, Phase separation in polysulfone-modified epoxy mixtures. Relationships between curing conditions, morphology and ultimate behavior., Polymer (2000).
[29] Y. Zhang, W. Shi, F. Chen, C. Han, Dynamically Asymmetric Phase Separation and Morphological Structure Formation in the Epoxy/Polysulfone Blends, Macromolecules 44 (2011) 7465.
[30] M. Rico, J. López, B. Montero, R. Bouza, F.J. Díez, Influence of the molecular weight of a modifier on the phase separation in an epoxy thermoset modified with a thermoplastic, European Polymer Journal 58 (2014) 125-134.
[31] S. Grishchuk, O. Gryshchuk, M. Weber, J. Karger-Kocsis, Structure and toughness of polyethersulfone (PESU)-modified anhydride-cured tetrafunctional epoxy resin: Effect of PESU molecular mass, Journal of Applied Polymer Science 123(2) (2012) 1193-1200.

[32] P. Jyotishkumar, J. Pionteck, R. Häßler, C. Sinturel, V. Mathew, S. Thomas, Effect of Cure Conditions on the Generated Morphology and Viscoelastic Properties of a Poly(acrylonitrile–butadiene–styrene) Modified Epoxy–Amine System, Industrial & Engineering Chemistry Research 51 (2012) 2586–2595.
[33] A. Saalbrink, A. Lorteije, T. Peijs, The influence of processing parameters on interphase morphology in polymer composites based on phase-separating thermoplast/epoxy blends, Composites Part A: Applied Science and Manufacturing 29(9–10) (1998) 1243-1250.
[34] J.S. Nakka, K.M.B. Jansen, L.J. Ernst, Tailoring the viscoelasticity of epoxy thermosets, Journal of Applied Polymer Science 128(6) (2013) 3794-3806.
[35] H. Tanaka, Viscoelastic phase separation, Journal of Physics: Condensed Matter 12(15) (2000) R207-R264.
[36] P. Jyotishkumar, C. Özdilek, P. Moldenaers, C. Sinturel, A. Janke, J. Pionteck, S. Thomas, Dynamics of Phase Separation in Poly(acrylonitrile-butadiene-styrene)-Modified Epoxy/DDS System: Kinetics and Viscoelastic Effects, The Journal of Physical Chemistry B 114(42) (2010) 13271-13281.
[37] Y. Liu, Polymerization-induced phase separation and resulting thermomechanical properties of thermosetting/reactive nonlinear polymer blends: A review, Journal of Applied Polymer Science 127(5) (2013) 3279-3292.
[38] Q. Guo, Thermosets: Structure, Properties, and Applications, Elsevier Science2017.
[39] E. Mathis, M.L. Michon, C. Billaud, P. Grau, A. Bocahut, C. Vergelati, D.R. Long, Thermoset modified with polyethersulfone: Characterization and control of the morphology, Journal of Polymer Science 58(8) (2020) 1177-1188.
[40] M.L. Williams, R.F. Landel, J.D. Ferry, The Temperature Dependence of Relaxation Mechanisms in Amorphous Polymers and Other Glass-forming Liquids, Journal of the American Chemical Society 77(14) (1955) 3701-3707.
[41] J.D. Ferry, Viscoelastic properties of polymers, 3rd Edition, John Wiley & Sons, Inc.1980.
[42] K.L. Hoy, C. Union Carbide, Solvents, D. Coatings Materials, Research, D. Development, The Hoy tables of solubility parameters, Union Carbide Corp., Solvents & Coatings Materials, Research & Development Dept., South Charleston, W. Va., 1985.
[43] B. Hammouda, S. Krueger, C.J. Glinka, Small Angle Neutron Scattering at the National Institute of Standards and Technology, Journal of Research of the National Institute of Standards and Technology 98(1) (1993) 31-46.
[44] G.L. Squires, Introduction to the Theory of Thermal Neutron Scattering, 3 ed., Cambridge University Press, Cambridge, 2012.
[45] V.F. Sears, Neutron scattering lengths and cross sections, Neutron News 3(3) (1992) 26-37.
[46] G. Beaucage, H.K. Kammler, S.E. Pratsinis, Particle size distributions from small-angle scattering using global scattering functions, Journal of Applied Crystallography 37(4) (2004) 523-535.
[47] M. Abramowitz, I.A. Stegun, Handbook of mathematical functions with formulas, graphs, and mathematical tables, US Government printing office1964.
[48] N. Clarke, T.C.B. McLeish, S.D. Jenkins, Phase Behavior of Linear/Branched Polymer Blends, Macromolecules 28(13) (1995) 4650-4659.
[49] P.J. Flory, Principles of Polymer Chemistry, Cornell University Press1953.
[50] M. Rubinstein, R.H. Colby, Polymer physics, Oxford university press New York2003.
[51] H.H. Winter, F. Chambon, Analysis of Linear Viscoelasticity of a Crosslinking Polymer at the Gel Point, Journal of Rheology 30(2) (1986) 367-382.
[52] B.S. Kim, T. Chiba, T. Inoue, Phase separation and apparent phase dissolution during cure process of thermoset/thermoplastic blend, Polymer 36(1) (1995) 67-71.
[53] B.S. Kim, T. Chiba, T. Inoue, A new time-temperature-transformation cure diagram for thermoset/thermoplastic blend: tetrafunctional epoxy/poly(ether sulfone), Polymer 34(13) (1993) 2809-2815.

[54] P.R. Couchman, F.E. Karasz, A Classical Thermodynamic Discussion of the Effect of Composition on Glass-Transition Temperatures, Macromolecules 11(1) (1978) 117-119.
[55] J.P. Pascault, R.J.J. Williams, Glass transition temperature versus conversion relationships for thermosetting polymers, Journal of Polymer Science Part B: Polymer Physics 28(1) (1990) 85-95.
[56] B.S. Kim, T. Chiba, T. Inoue, Morphology development via reaction-induced phase separation in epoxy/poly(ether sulfone) blends: morphology control using poly(ether sulfone) with functional end-groups, Polymer 36(1) (1995) 43-47.
[57] J.T. Cabral, J.S. Higgins, Spinodal nanostructures in polymer blends: On the validity of the Cahn-Hilliard length scale prediction, PROGRESS IN POLYMER SCIENCE 81 (2018) 1-21.
[58] I.G. Voigt-Martin, K.-H. Leister, R. Rosenau, R. Koningsveld, Kinetics of phase separation in polymer blends for deep quenches, Journal of Polymer Science Part B: Polymer Physics 24(4) (1986) 723-751.
[59] J.W. Cahn, J.E. Hilliard, Free Energy of a Nonuniform System. I. Interfacial Free Energy, The Journal of Chemical Physics 28(2) (1958) 258-267.
[60] E. Manias, L.A. Utracki, Thermodynamics of Polymer Blends, in: L.A. Utracki, C.A. Wilkie (Eds.), Polymer Blends Handbook, Springer Netherlands, Dordrecht, 2014, pp. 171-289.
[61] I.M. Lifshitz, V.V. Slyozov, The kinetics of precipitation from supersaturated solid solutions, Journal of Physics and Chemistry of Solids 19(1) (1961) 35-50.
[62] P.G. de Gennes, Dynamics of fluctuations and spinodal decomposition in polymer blends, The Journal of Chemical Physics 72(9) (1980) 4756-4763.
[63] G. Julien, Dynamics in polymer blends and polymer-solvent blends close to the glass transition, Université Claude Bernard - Lyon I, 2014.
[64] P.E. Rouse, A Theory of the Linear Viscoelastic Properties of Dilute Solutions of Coiling Polymers, The Journal of Chemical Physics 21(7) (1953) 1272-1280.
[65] C. Ligoure, L. Leibler, Thermodynamics and kinetics of grafting end-functionalized polymers to an interface, Journal De Physique 51(12) (1990) 1313-1328.
[66] X. Cheng, Q. Wu, S.E. Morgan, J.S. Wiggins, Morphologies and mechanical properties of polyethersulfone modified epoxy blends through multifunctional epoxy composition, Journal of Applied Polymer Science 134(18) (2017) 134.
[67] T.H. Oyama, J.J. Lesko, J.P. Wightman, Interdiffusion at the interface between poly(vinylpyrrolidone) and epoxy, Journal of Polymer Science Part B: Polymer Physics 35(2) (1997) 331-346.
[68] J. Jose, K. Joseph, J. Pionteck, S. Thomas, PVT Behavior of Thermoplastic Poly(styrene-co-acrylonitrile)-Modified Epoxy Systems: Relating Polymerization-Induced Viscoelastic Phase Separation with the Cure Shrinkage Performance, The Journal of Physical Chemistry B 112(47) (2008) 14793-14803.
[69] P. Jyotishkumar, J. Pionteck, C. Özdilek, P. Moldenaers, U. Cvelbar, M. Mozetic, S. Thomas, Rheology and pressure–volume–temperature behavior of the thermoplastic poly(acrylonitrile-butadiene-styrene)-modified epoxy-DDS system during reaction induced phase separation, Soft Matter 7(16) (2011) 7248-7256.
[70] P. Jyotishkumar, A. George, J. Pionteck, S. Thomas, Investigation of Cure Reaction, Rheology, Volume Shrinkage and Thermomechanical Properties of Nano-TiO2 Filled Epoxy/DDS Composites, Journal of Polymers 2013 (2013) 183463.
[71] E. Mathis, Thermoplastic toughened thermoset composites: Control of morphology, in relation with applicative properties, PhD thesis (2020) 115-143.

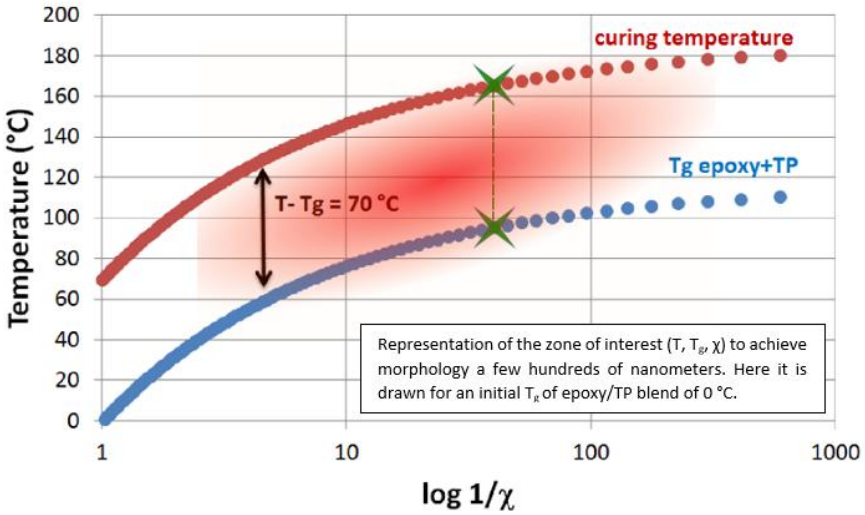

for TOC, Mathis, Michon, Billaud, Vergelati, Clarke, Jestin, Long